Published by IOP Publishing for SISSA
Received: *August 20, 2008*
Accepted: *October 17, 2008*
Published: *October 27, 2008*

Handling jets + missing E_T channel using inclusive m_{T2}

Mihoko M. Nojiri
Theory Group, KEK and the Graduate University for Advanced Study (SOUKENDAI), Oho 1-1, Tukuba, Ibaraki, 305-0801, Japan, and
Institute for the Physics and Mathematics of the Universe (IPMU), University of Tokyo, 5-1-5 Kashiwa-noHa, Kashiwa, Chiba, 277-8568, Japan
E-mail: nojiri@post.kek.jp

Kazuki Sakurai
Department of Physics, Nagoya University, Nagoya, Aichi, 464-8602, Japan
E-mail: sakurai@eken.phys.nagoya-u.ac.jp

Yasuhiro Shimizu
Tohoku University International Advanced Research and Education Organization, Institute for International Advanced Interdisciplinary Research, Sendai, Miyagi 980-8578, Japan
E-mail: shimizu@tuhep.phys.tohoku.ac.jp

Michihisa Takeuchi
Yukawa Institute for Theoretical Physics, Kyoto University, Kyoto 606-8502, Japan, and
Theory Group, KEK, Oho 1-1, Tukuba, Ibaraki, 305-0801, Japan
E-mail: tmichihi@post.kek.jp

Abstract: The ATLAS and CMS experiments at the Large Hadron Collider (LHC) may discover the squarks ($\tilde{q}$) and gluino ($\tilde{g}$) of the minimal supersymmetric standard model (MSSM) in the early stage of the experiments if their masses are lighter than 1.5 TeV. In this paper we propose the sub-system m_{T2} variable ($m_{T2}^{\rm sub}$), which is sensitive to the gluino mass when $m_{\tilde{q}} > m_{\tilde{g}}$. Using it with the inclusive m_{T2} distribution proposed earlier, $\tilde{q}$ and $\tilde{g}$ masses can be determined simultaneously in the early stage of the experiments. Results of Monte Carlo simulations at sample MSSM model points are presented both for signal and background.

Keywords: Supersymmetric Standard Model, Hadronic Colliders, Jets.

JHEP10(2008)100

Contents

JHEP10(2008)100

1. Introduction

Supersymmetry (SUSY) provides an elegant solution to the hierarchy problem in the Standard Model (SM) Higgs sector [1 – 3]. It predicts a set of new particles containing spin 0 sfermions and spin 1/2 gauginos and higgsinos. If R parity is conserved, the lightest supersymmetric particle (LSP), which is often the lightest neutralino, is stable and a good dark matter candidate. The thermal relic density of the LSP can be consistent with the cold dark matter density of our Universe.

The ATLAS and CMS experiments at the CERN Large Hadron Collider (LHC) may discover the SUSY particles in the early stage of data collection. The missing momentum carried by the stable LSP becomes an important signature of the sparticle production. Current studies show that an integrated luminosity of around $1\,\mathrm{fb}^{-1}$ is enough to find sparticle production if the squark and gluino masses are below 1.5 TeV and the mass difference between the LSP and squark/gluino is large.

We do not yet have many clues on the sparticle mass scale, although the current measurements of flavor changing neutral current (FCNC) give stringent constraints on the relation among sfermion masses unless they are extremely heavy. Once we have seen signs of SUSY at the LHC, we should use direct evidence to determine the SUSY particle masses, from which we may determine the sparticle mass relations. Various methods have been developed for spaticle mass determination from event kinematics. The invariant mass distributions of various exclusive channels are known to be very useful [4 – 9]. By combining the measured endpoints of the distributions of the relatively clean and long cascade decay channels involving charginos ($\tilde{\chi}_i^{\pm}$), neutralinos ($\tilde{\chi}_i^0$) and sleptons ($\tilde{l}$), such as the opposite sign same flavor lepton signal arising from $\tilde{q} \to \tilde{\chi}_2^0 q \to \tilde{l} q l \to \tilde{\chi}_1^0 q l l$, one can determine

not only the masses of the squark and gluino, but also the neutralino and slepton masses arising from their cascade decays. The exact relations among momenta of visible particles from a cascade decay are also useful [10 – 13]. For some cases, the decay kinematics can be solved event by event to obtain the sparticle masses in the decay cascade.

Another important quantity is the m_{T2} variable, which is calculated from two visible momenta $p_{\rm vis}^{(i)}(i=1,2)$ and the missing transverse momentum $\not{\mathbf{E}}_T$ as in eq. (1.1) [14, 15],

$$m_{T2} = \min_{\not{\mathbf{E}}_T = \not{\mathbf{p}}_T^{(1)} + \not{\mathbf{p}}_T^{(2)}} \left[\max \left\{ m_T(p_{\rm vis}^{(1)}, \not{\mathbf{p}}_T^{(1)}; M_{\rm test}), m_T(p_{\rm vis}^{(2)}, \not{\mathbf{p}}_T^{(2)}; M_{\rm test}) \right\} \right]. \qquad (1.1)$$

Here, $p_{\rm vis}^{(i)}(i=1,2)$ is the sum of momenta of the particles in the visible system i which is a set of visible decay products from a parent particle i. $M_{\rm test}$ is an arbitrary mass parameter called the test LSP mass.

The quantity is bounded above by the mass of the heavier of the initially produced sparticles if we set $M_{\rm test} = m_{\rm LSP}$. This property of the m_{T2} is useful for determining the sparticle masses. For example, for the process $pp \to \tilde{q}_R \tilde{q}_R \to jj\chi_1^0\chi_1^0$ studied in [16, 17], the events are populated near the m_{T2} endpoint, which is very clearly visible and coincides with $m_{\tilde{q}_R}$.

It was pointed out recently that the endpoint of the m_{T2} distribution $m_{T2}^{\rm end}$ as a function of $M_{\rm test}$ has a kink at the true LSP mass in the case that the invariant mass of the visible system $m_{\rm vis}$ (which consists of jets and leptons) can range [18 – 24]. The kink arises because the derivative of $m_{T2}^{\rm end}$ with respect to a test LSP mass differs depending on the $m_{\rm vis}$, while $m_{T2}^{\rm end}$ cannot be above the parent sparticle masses $\max\{m_1, m_2\} \equiv M$ at $M_{\rm test} = m_{\rm LSP}$, so every trajectory that an event makes on the $m_{T2} - M_{\rm test}$ plane passes or goes below the point $(m_{T2}, M_{\rm test}) = (M, m_{\rm LSP})$. The LSP mass and gluino mass may be reconstructed from $M_{\rm test}$ and the $m_{T2}^{\rm end}$ value at the kink position. The mass determination has been demonstrated in the four jets and $\not{E}_T$ channel at a certain MSSM model point in which $\tilde{g}$ decays dominantly via $\tilde{g} \to \tilde{q}q \to \tilde{\chi}_1^0 qq$ and $\tilde{q}$ is heavy [21]. This shows that short hadronic decay chains can also contribute to sparticle mass determination.

To make use of the SUSY events fully in the early stage of the LHC, it is useful to define the m_{T2} variable in an inclusive manner without any specification of decay modes. This is because a squark and a gluino may decay into a mode with more than two jets in the final state. For example, the decay modes $\tilde{g} \to t\bar{t}\tilde{\chi}_1^0$ and $tb\tilde{\chi}_1^\pm$ have large branching ratios in large mSUGRA parameter regions, because the scalar top and the scalar bottom tend to have masses much lighter than the first generation squark masses.

In the previous paper, we therefore define an inclusive m_{T2} variable using a hemisphere method [22]. The inclusive m_{T2} is defined in two steps. In the first step, we divide jets in each event into two hemispheres [25, 26]. This is normally done by associating the jets with two leading axes which are initially taken as the two leading jets in the event. The sum of the jet momenta assigned in a hemisphere is called a hemisphere momentum $p_{\rm hemi}^{(i)}(i=1,2)$. In the next step, a stransverse mass m_{T2} is calculated using eq. (1.1) with $p_{\rm hemi}^{(i)}$ taken as $p_{\rm vis}^{(i)}$. The inclusive m_{T2} as defined above carries the information on the parent sparticle masses $\max\{m_1, m_2\}$, if the hemisphere algorithm groups the decay products from the particle 1 and 2 into two different hemispheres correctly. It is shown that a parent squark mass $m_{\tilde{q}}$ can be obtained from $m_{T2}^{\rm end}$ in the case of $m_{\tilde{q}} > m_{\tilde{g}}$. Moreover, the $m_{T2}^{\rm end}$ as a function of

JHEP10(2008)100

a test LSP mass still has a kink at the true LSP mass. The inclusive m_{T2} distribution is also useful for discriminating model parameters and discussed extensively in [27].

In this paper, we propose a "sub-system m_{T2}", $m_{T2}^{\rm sub}$. It is defined as an inclusive m_{T2} variable, but the highest p_T jet is removed before the hemisphere reconstruction. The definition is inspired by an observation that the squark decays via $\tilde{q} \to \tilde{g}$ or $\tilde{q} \to \tilde{\chi}^{\pm}, \tilde{\chi}^0$ produce a high p_T jet if $m_{\tilde{q}}$ is sufficiently larger than $m_{\tilde{g}}$, $m_{\tilde{\chi}^{\pm}}$ and $m_{\tilde{\chi}^0}$. In the case that the jet from the squark decay is identified, the remaining system is either gluino-gluino or gluino-neutralino/chargino for $\tilde{q}\tilde{g}$ co-production, so $m_{T2}^{\rm sub}({\rm end}) = m_{\tilde{g}}$. By studying several model points we provide convincing cases that *both* $m_{\tilde{q}}$ and $m_{\tilde{g}}$ are estimated using $m_{T2}^{\rm end}$ and $m_{T2}^{\rm sub,end}$. We also calculate background distributions coming from the productions $t\bar{t} + n$ jets, $W + n$ jets and $Z + n$ jets using `ALPGEN` [28, 29] with MLM matching. We find that the signal to noise ratio (S/N) is large especially for the events near the m_{T2} endpoint, which are most sensitive to squark and gluino masses.

The importance of matrix element (ME) corrections to SUSY processes have been emphasized recently [30 – 32]. We provide an estimate of the size of the matrix element correction to the signal m_{T2} distributions using `MadGraph` [33]. We find that the signal m_{T2} distributions are not significantly modified by the SUSY matrix element corrections near the endpoint of the m_{T2} distributions.

This paper is organized as follows. In section 2, we describe the sub-system m_{T2}. We show parton level m_{T2} and $m_{T2}^{\rm sub}$ distributions, and discuss reconstruction efficiencies of the SUSY decay cascades using a hemisphere algorithm at our sample model point. The jet level distributions using `HERWIG` [34] with simple detector simulator `AcerDET` [35] are given in section 3. We study the SM background distributions generated by `ALPGEN` in section 4. Section 5 is devoted to the conclusions.

In appendix A, we describe the condition that $m_{T2}^{\rm end}$ coincides with the mass of the heavier of the initially produced squarticles. The effects of the matrix element corrections to m_{T2} distributions are studied in appendix B.

2. The sub-system inclusive m_{T2} ($m_{T2}^{\rm sub}$) — parton level analysis

At the LHC, squarks and gluinos are copiously produced via $\tilde{q}\tilde{q}, \tilde{q}\tilde{g}$ and $\tilde{g}\tilde{g}$ production processes. Each of them decays into visible objects and a LSP. If the visible systems are correctly grouped, the inclusive m_{T2} with the correct $p_{\rm vis}^{(i)}$ defined as eq. (1.1) can be calculated. In that case, the important property is[1]

$$m_{T2}^{\rm end} = \max\{m_1, m_2\}. \tag{2.1}$$

Here, $m_{T2}^{\rm end}$ denotes the endpoint of the m_{T2} distribution and m_1 and m_2 denote the masses of the produced parent particles. In this section, the test mass is taken as the true LSP mass ($M_{\rm test} = m_{\rm LSP}$).

In the case of $m_{\tilde{q}} \gg m_{\tilde{g}}$, squark-gluino and gluino-gluino production events are dominant SUSY production processes. They give the different m_{T2} endpoints: $m_{\tilde{q}}$ and $m_{\tilde{g}}$. For

[1]The endpoint for $\tilde{q}\tilde{g}$ production events is given by $\max\{m_{\tilde{q}}, m_{\tilde{g}}\}$ unless the LSP mass is too close to $m_{\tilde{g}}$, which is satisfied in the typical mass spectrum. More details are discussed in appendix A.

JHEP10(2008)100

	m_0	A_0	$m_{\tilde{q}}$	$m_{\tilde{g}}$	$m_{\rm LSP}$	μ
a	1400	−1400	1516	795.7	107.9	180
b	1200	−1200	1342	785.0	107.4	180
c	1100	−1100	1257	779.5	107.1	180
d	1000	−1000	1175	773.2	106.8	180
e	820	−750	1035	761.7	106.1	180
f	600	−650	881.0	745.4	107.8	190

Table 1: Some of the mass parameters of our model points. We take the scalar masses of sfermions and gaugino masses to be universal. We tune the higgsino mass parameter μ by allowing non-universal GUT scale Higgs masses parameters so that $\Omega h^2 \sim 0.1$. All mass parameters are given in GeV.

the squark-gluino production events, a squark decays dominantly into a gluino (or another lighter sparticle) and a jet. If we can identify the jet, all other elements of the system make up a sub-system that may be considered as a gluino-gluino (or gluino-the other sparticle) system. We introduce the variable $m_{T2}^{\rm sub}$ (sub-system m_{T2}), which is m_{T2} calculated for the sub-system. The missing transverse momentum is taken as the same as for the whole system since the sum of the two LSP momenta is required for the calculation of m_{T2}. The expected endpoint of $m_{T2}^{\rm sub}$ is $m_{\tilde{g}}$.

Practically, we define the sub-system as the system with the highest p_T jet removed. If the highest p_T jet is from a decay chain of a squark, the endpoint of $m_{T2}^{\rm sub}$ is expected as,

$$m_{T2}^{\rm sub,end} = \min\{m_1, m_2\}. \tag{2.2}$$

We now show parton level m_{T2} and $m_{T2}^{\rm sub}$ distributions at our sample model points. Here, we take the model points "a - f" listed in table 1 with the GUT scale gaugino mass $M_{1/2} = 300\,\text{GeV}$ and $\tan\beta = 10$. The GUT scale sfermion mass m_0 is 600 GeV at point f and 1400 GeV at point a. The gluino masses at these points are approximately the same, while squark masses range from $\sim 900\,\text{GeV}$ (at point f) to $\sim 1500\,\text{GeV}$ (at point a). The GUT scale Higgs masses are tuned so that the μ parameters are small $\sim 180\,\text{GeV}$. The relation $\mu \sim M_1$ results in a thermal relic density of the LSP that is consistent with the observed cold dark matter density of our universe [36 – 38].[2] Some of the branching ratios of the 1st generation squarks are given in table 2. We calculate the masses and the branching ratios at these model points using `ISAJET` [39], and the mass parameters are interfaced to `HERWIG` [34] using `ISAWIG` [40]. The cross sections are calculated using `HERWIG`. Note that the values of m_0 and $M_{1/2}$ in table 1 are within the discovery reach in mSUGRA for the ATLAS and CMS experiments at $\int dtL = 1\,\text{fb}^{-1}$.

The squark production cross section reduces quickly with increasing first generation squark masses. The total SUSY production cross section varies more than a factor of two from point a to point f. The difference comes mostly from the decrease of $\sigma(\tilde{q}\tilde{g})$. In particular, the production cross section involving at least one first generation squark is only 0.46 pb at point a and 4.34 pb at point f. The gluino-gluino production cross section

[2]The choice of the μ parameter does not affect m_{T2} distributions discussed in this paper.

point	$m_{\tilde{u}_L}$	$Br(\tilde{u}_L \to \tilde{g}u)$	$Br(\tilde{u}_R \to \tilde{g}u)$	σ(SUSY)(pb)	$\sigma(\tilde{q})$ (pb)
a	1516	0.71	0.93	4.91	0.46
b	1342	0.68	0.92	5.35	0.79
c	1257	0.66	0.91	5.84	1.07
d	1175	0.62	0.90	6.15	1.40
e	1035	0.53	0.96	7.31	2.36
f	881	0.31	0.71	9.49	4.34

Table 2: Some relevant branching ratios of squarks are calculated using ISAJET. The total SUSY production cross section and the cross section involving at least one first generation squark estimated using HERWIG are also given.

also becomes reduced because t-channel squark exchange is suppressed. Chargino and neutralino production is important at point a.

The squark decays dominantly into gluino and a jet (See table 2). The squark branching ratio into the gluino is dominant except at point f. For points a to c, the mass difference between squark and gluino is significantly larger than half of the gluino mass. Therefore, a jet from a squark decay is likely to be the highest p_T jet in the event. Jets from the other squark decay modes such as $\tilde{q} \to \tilde{\chi}_i^0 j$ and $\tilde{\chi}^{\pm} j$ have p_T which is even higher than that of $\tilde{q} \to \tilde{g} j$ on average.

To define the inclusive m_{T2} and $m_{T2}^{\rm sub}$ distributions, we group jets in an event into two "visible objects". For this purpose, we adopt the hemisphere method in refs. [25, 26]. For each event, two hemispheres are defined and high p_T jets are assigned to one of the hemispheres as follows:

1. Each hemisphere is defined by an axis $p_{\rm hemi}^{(i)}$ $(i = 1, 2)$, which is the sum of the momenta of the selected high p_T objects belonging to the hemisphere i.

2. A high p_T object k belonging to a hemisphere i satisfies the following conditions:

$$d(p_k, p_{\rm hemi}^{(i)}) < d(p_k, p_{\rm hemi}^{(j)}), \tag{2.3}$$

where the function d is defined by

$$d(p_k, p_{\rm hemi}^{(i)}) = (E_{\rm hemi}^{(i)} - |\mathbf{p}_{\rm hemi}^{(i)}| \cos\theta_{ik}) \frac{E_{\rm hemi}^{(i)}}{(E_{\rm hemi}^{(i)} + E_k)^2} \tag{2.4}$$

Here θ_{ik} is the angle between $\mathbf{p}_{\rm hemi}^{(i)}$ and $\mathbf{p}_k$.

For our m_{T2} analysis in this paper, the selected objects are jets with $p_{Ti} > 50\,\text{GeV}$ and $|\eta_i| < 3$. We do not include the jets with $p_T \leq 50\,\text{GeV}$ nor $|\eta_i| > 3$ to avoid contaminations from initial state radiations. For $m_{T2}^{\rm sub}$, we do not include the highest p_T jet in the selected objects.

To find the $p_{\rm hemi}^{(i)}$, we adopted the algorithm discussed in refs. [25]:

1. We first take the highest p_T object with momentum p_1 and the object i which has the largest $p_{Ti} \times \Delta R(1, i)$, where $\Delta R(i, j) = \sqrt{(\eta_i - \eta_j)^2 + (\phi_i - \phi_j)^2}$.

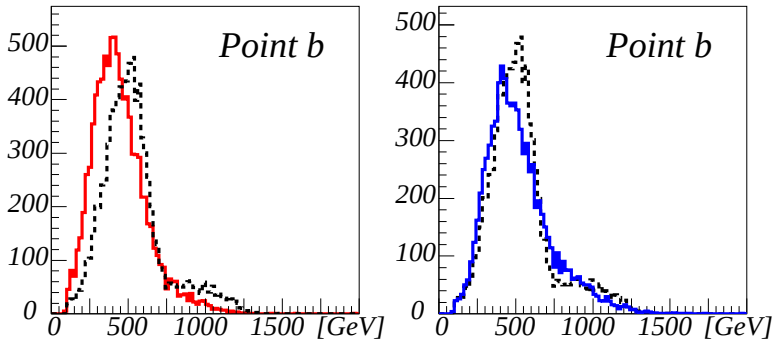

Figure 1: Various parton level $m_{T2}^{\rm sub}$ distributions at point b. The left plot, a solid line: the $m_{T2}^{\rm sub}$ distribution. The right plot, a solid line: a $\tilde{m}_{T2}^{\rm sub}$ distribution, which is a m_{T2} variables but calculated after subtracting the highest p_T object from the hemisphere momenta. Dotted lines, $m_{T2}^{\rm sub}$(true) distributions, which uses generator information for the hemisphere assignment. Arbitrary normalizations are used for the y-axes. See text for details.

2. We regard p_1 and p_i as two seeds of the initial hemisphere axes, and assign the other objects to one of the two axes.

3. We recalculate the hemisphere axes. We perform iterations until the assignment converges. Once $p_{\rm hemi}$'s are determined, one can calculate m_{T2} by using eq. 1.1 with taking $p_{\rm hemi}$ as $p_{\rm vis}$.

In this section, we study *parton level events*. The momenta of quarks and gluons from sparticle decays are extracted from HERWIG event records, and only $\tilde{q}$-$\tilde{q}^{(*)}$, $\tilde{q}^{(*)}$-$\tilde{g}$ and $\tilde{g}$-$\tilde{g}$ productions are included in the figures. When a sparticle decays into $W^{\pm}$,Z^0, and t, we further follow their decays. Note that each parton is in general off-shell when they are created from a sparticle decay, and we do not follow parton shower evolutions after that. We do not include partons from initial state radiations. These effects will be taken into account in particle level MC simulations in the next section.

For the calculation of the $m_{T2}^{\rm sub}$, we remove the highest p_T jet before the hemisphere assignment to obtain the $p_{\rm hemi}$'s. As an alternative definition, we can remove the highest p_T jet from the $p_{\rm hemi}$'s after the hemisphere assignment, and $\tilde{m}_{T2}^{\rm sub}$ denotes this alternative m_{T2} in the following.

We now compare $m_{T2}^{\rm sub}$ and $\tilde{m}_{T2}^{\rm sub}$ at point b in figure 1. In the left plot, we show the $m_{T2}^{\rm sub}$ distribution in the solid line. In the right plot, the solid line shows the $\tilde{m}_{T2}$ distribution. In each plot, the dotted line shows the 'true distribution' $m_{T2}^{\rm sub}$(true), in which the $p_{\rm vis}^{(i)}$ consists of the momenta of decay products from a parent particle i except for the highest p_T parton using the generator information. This is an ideal distribution when the assignment of the visible systems is perfect. Note that the highest p_T jet is not always from a $\tilde{q}$ decay. Even in the distribution of $m_{T2}^{\rm sub}$(true), two endpoints can be seen, the lower is at the gluino mass and the higher is at the squark mass.

The endpoint at the gluino mass is more clearly visible for the $m_{T2}^{\rm sub}$ than for the $\tilde{m}_{T2}^{\rm sub}$ distribution. The improvement in $m_{T2}^{\rm sub}$ distribution may be explained as follows. At point b, a parton from $\tilde{q} \to q\tilde{g}$ has a large open angle to the gluino decay products on

JHEP10(2008)100

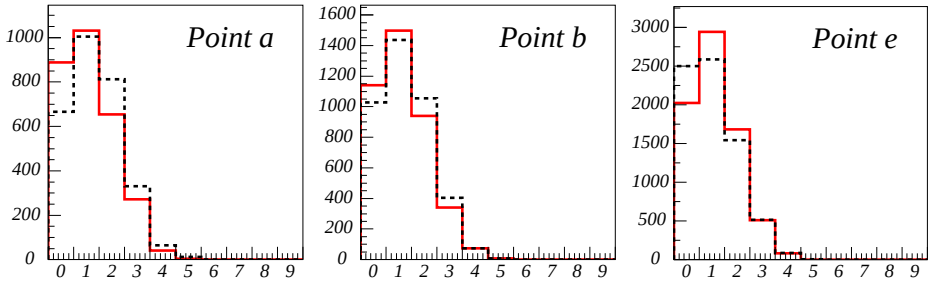

Figure 2: The distributions of the number of partons assigned to an incorrect hemisphere at point a (left), b (middle) and e (right). In all figures, solid (dashed) histograms correspond to the case that the highest p_T parton is removed before (after) the hemisphere assignment. Arbitrary normalizations are used for the y-axes. See text for details.

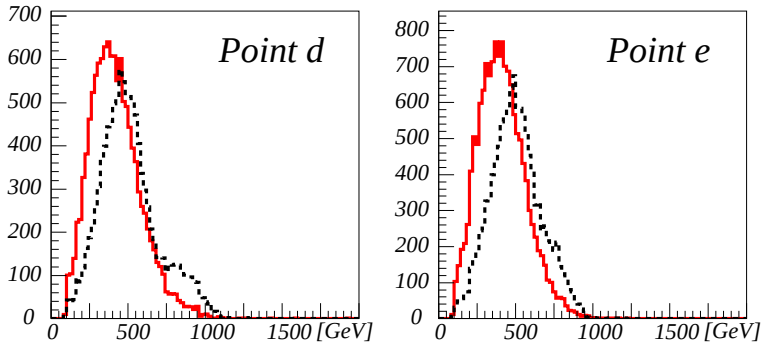

Figure 3: The $m_{T2}^{\rm sub}$ distributions (solid) and the $m_{T2}^{\rm sub}$(true) distributions (dashed) for squark-gluino co-production events at points d and e. Arbitrary normalizations are used for the y-axes.

average. The event effectively has three axes: the two momenta of the two gluino decay products and the momentum of the extra parton from squark decay. The assumption of the hemisphere algorithm that events must have two axes may lead to an incorrect hemisphere assignment. Removing the highest p_T parton before the hemisphere assignment therefore makes the kinetic endpoints more visible.

The successful endpoint reconstruction shows that the hemisphere algorithm reconstructs a total visible momentum of a squark/gluino decay more or less correctly. One can check this explicitly by counting the number of partons assigned to an incorrect hemisphere. (figure 2). The solid (dashed) histograms correspond to the distributions of the number of mis-reconstructed partons for the case that the highest p_T parton is removed before (after) the hemisphere assignment. The improvement achieved by removing the highest p_T parton before the hemisphere assignment is clearly seen at point a (the left plot). At this point, $m_{\tilde{q}} = 1516\,\text{GeV}$ and $m_{\tilde{b}} = 796\,\text{GeV}$, so the parton from the squark decay should have p_T of the order of several hundred GeV. We also see mild improvement at point b (the middle plot). At point e (the right plot), the squark and gluino masses are close, $(m_{\tilde{q}} - m_{\tilde{g}})/m_{\tilde{g}} = 0.36$. In this case, removing the highest p_T jet before the hemisphere assignment leads to the slightly worse reconstruction efficiency. The number of mis-reconstructed partons is either 0 or one for more than half of the events in figure 2.

JHEP10(2008)100

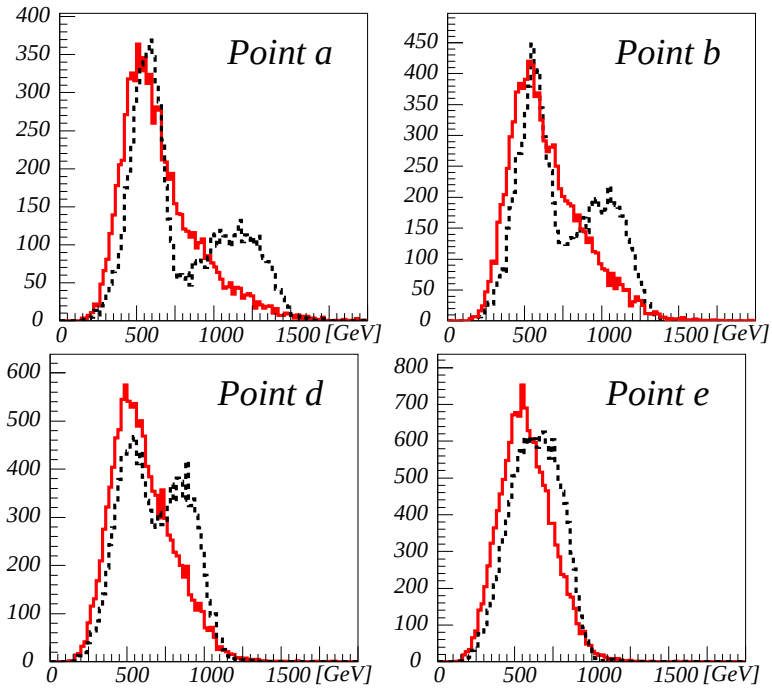

Figure 4: The parton level m_{T2} distributions at points a, b, d and e. The solid lines correspond to the distributions using the hemisphere algorithm, while the dotted lines correspond to those with correct parton assignments obtained by using the generator information. Arbitrary normalizations are used for the y-axes.

If the highest p_T parton does not arise from $\tilde{q}$ decay, the gluino endpoint cannot be reconstructed even for squark-gluino production events. The probability strongly depends on the model parameters. In figure 3 we show the $m_{T2}^{\rm sub}$ distributions for only squark-gluino co-production events at points d (left) and e (right). The gluino endpoint can be seen around 750 GeV from the $m_{T2}^{\rm sub}$ distribution at point d, which is close to that of the $m_{T2}^{\rm sub}$(true) distribution shown in the dotted line. However, at point e, even in the $m_{T2}^{\rm sub}$(true) distribution we cannot see the clear structure at the gluino mass.

The difference between the $m_{T2}^{\rm sub}$ and $m_{T2}^{\rm sub}$(true) distributions at points d and e may be explained as follows. At point d, $(m_{\tilde{q}} - m_{\tilde{g}})/m_{\tilde{g}} = 0.52$, and the energy of the parton from the squark decay is bigger than that from the gluino on average. This is why $m_{T2}^{\rm sub}$ shows clear gluino endpoints at point d. In contrast, $(m_{\tilde{q}} - m_{\tilde{g}})/m_{\tilde{g}} = 0.36$ at point e. The $m_{\tilde{q}} - m_{\tilde{g}}$ is not large enough, and it is not likely that the parton from $\tilde{q} \to \tilde{g}q$ has significantly high p_T compared with those coming from the gluino decays. This is why the $m_{T2}^{\rm sub}$(true) distribution does not show the endpoint at the gluino mass, it could be a problem to extract the gluino mass from the $m_{T2}^{\rm sub}$ distribution. However, the $m_{T2}^{\rm sub}$ distribution of $\tilde{q}\tilde{g}$ production is significantly smeared towards the lower m_{T2} value. In the actual situation, the contribution from gluino-gluino pair productions would be added, and the $m_{T2}^{\rm sub}$ distribution would have the endpoint at the gluino mass. We will see in the next section that the contamination from squark-gluino production is not serious.

For completeness, we show the parton level m_{T2} distributions at points a, b, d and

JHEP10(2008)100

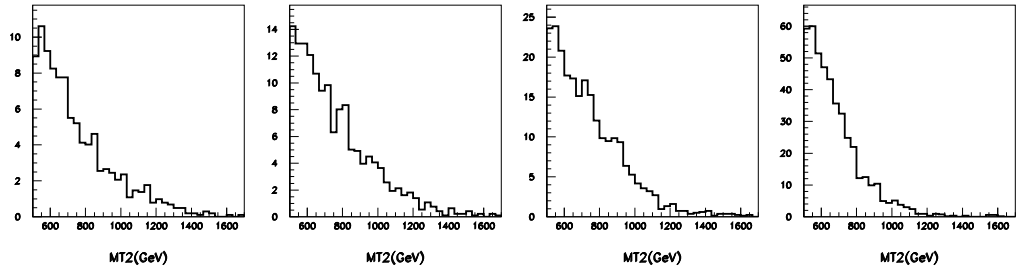

Figure 5: The inclusive m_{T2} destributions at points a b, d and f (from left to right). The up squark mass is 1516, 1342, 1175, 881 GeV from left to right, respectively. Unit of y-axes is events/bin/1 fb^{-1}.

e in figure 4 to emphasize the difference between m_{T2} and $m_{T2}^{\rm sub}$ distributions. The solid histograms are the m_{T2} distributions using the hemisphere algorithm, while the dotted histograms correspond to the m_{T2}(true) distributions which are obtained by assigning the partons arising from a parent particle i to hemisphere i using generator information. At points a, b and d, the m_{T2}(true) distribution has two peaks. The peak at the lower m_{T2} value comes from gluino-gluino production, while the peak at higher m_{T2} corresponds to the squark-gluino and squark-squark productions. The endpoint of the distributions coincides with squark mass. The double peak structure cannot be seen in the distributions of m_{T2}, but the endpoints are the same as that of m_{T2}(true).

The slope of the distribution near the endpoint becomes flatter with increasing squark mass as can be seen from the distributions at points a, b, and d. In particular, the existence of a high p_T parton from squark decay leads to some confusions in the hemisphere algorithm at point a, and a careful study of the distribution would be required to extract the squark mass from the fit. The peak of the m_{T2} distribution coincides with the lower m_{T2}(true) peak. The events near the peak come from gluino pair productions at points a, b, and d. In principle, the position of the peak contains the gluino mass information. However, this is not easy to observe because the SM background may also be large in this region. At point e, although the endpoints of the m_{T2} and m_{T2}(true) distributions are consistent, the squark and gluino masses are too close for the two peak structure to be seen.

3. The MC simulation of the signal

We have shown that the endpoints of m_{T2} and $m_{T2}^{\rm sub}$ distributions carry the information on squark and gluino masses using parton level events. In this section we study the events produced by a parton shower Monte Carlo `HERWIG` (in the particle level) with a detector simulator `AcerDET` under the set of cuts to reduce the standard model backgrounds. The simple snowmass cone algorithm implemented in `AcerDET` is used for finding jets and we set the cone size $R = 0.4$.

We apply the following cuts to the events.

- Jet p_T cuts: $n_{50} \equiv N_{\rm jet}(p_T > 50\ {\rm GeV}) \geq 4$, $n_{100} \equiv N_{\rm jet}(p_T > 100\ {\rm GeV}) \geq 1$.

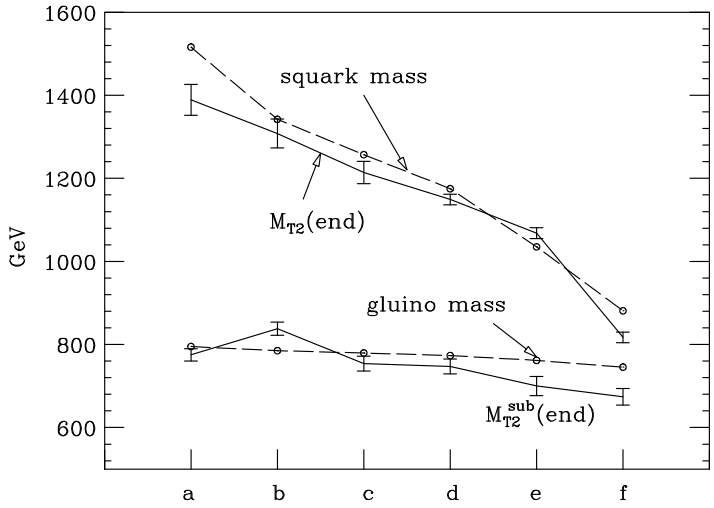

Figure 6: The fitted m_{T2} and $m_{T2}^{\rm sub}$ endpoints (solid lines) and $m_{\tilde{q}}$ and $m_{\tilde{g}}$ (dashed lines) at each model point. The bars show the size of statistical errors for 50,000 SUSY events.

- $M_{\rm eff}(\equiv \sum_{p_T^{\rm jet}>50{\rm GeV}} p_T + \not{E}_T) > 500\,{\rm GeV}$
- Transverse sphericity: $S_T > 0.2$.
- Missing Transverse momentum:$\not{E}_T > 200\,{\rm GeV}$, $\not{E}_T > 0.2 M_{\rm eff}$.
- No isolated lepton with $p_T > 20\,{\rm GeV}$.

These cuts are similar to the standard SUSY cuts in the ATLAS TDR [6], except for our tighter $\not{E}_T$ cut. We veto events with isolated leptons because a hard lepton might be assoicated with a hard neutrino. If there is a hard neutrino in an event, $p_{\rm Tmiss}$ of the event may not be the sum of the transverse momenta of LSPs. In that case, the endpoint of the m_{T2} distribution might be smeared.

We first show the m_{T2} distributions for our model points. The m_{T2} distributions for $m_{\rm test} = 10\,{\rm GeV}$ under the SUSY cuts are shown in figure 5.[3] For each point, we have generated 50,000 SUSY events and the distribution is scaled to correspond to $\int dt\mathcal{L} = 1\,{\rm fb}^{-1}$ of luminosity.

The endpoint of the m_{T2} distribution is roughly at $\sim m_{\tilde{q}}$. We fit the distributions to linear functions

$$\begin{aligned} f(m) &= a(m - m_{T2}^{\rm end}) + c \qquad && ({\rm for}\ \ m < m_{T2}^{\rm end}) \\ &= b(m - m_{T2}^{\rm end}) + c \qquad && ({\rm for}\ \ m > m_{T2}^{\rm end}), \end{aligned} \tag{3.1}$$

and the fitted $m_{T2}^{\rm end}$ values are shown in figure 6. Here, the statistical errors shown in bars correspond to 50,000 total SUSY events. The obtained $m_{T2}^{\rm end}$ and $m_{\tilde{q}}$ are consistent except at points a and f. For point f, the squark and gluino masses are too close, and it is natural

[3]We set $m_{\rm test}$ small as we do not know the LSP mass initially.

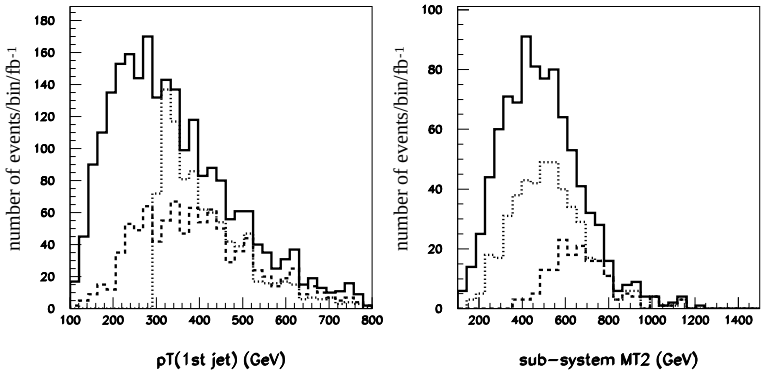

Figure 7: The p_T distributions of the highest p_T jet (left) among the jets with $|\eta| < 3$, and the distributions of the $m_{T2}^{\rm sub}$ (right) at point a. The dashed lines show the contributions from the events with $n_{300} = 1$ and the dotted lines show the contributions from the events with $n_{\tilde{q}} = 1$. The standard SUSY cuts are applied for all plots, and $m_{\rm test} = 10\,{\rm GeV}$. Unit of y-axes is events/bin/1 fb^{-1}.

that the endpoint fall at weighted mean of gluino and squark masses. For point a, due to the very large mass difference between squark and gluino, the hemisphere method involving the highest p_T jet does not work perfectly.

Note that there is some ambiguity in choosing a fitting region. For example, for point a, the distribution consists of the two components, one arising from the gluino-gluino production with the endpoint around 800 GeV and the other from the squark-gluino production with the endpoint around 1400 GeV. We fit the distribution above $m_{T2} > 1000\,{\rm GeV}$ for this point. If we did the same fit at point f (the right plot), we might fit the mis-reconstructed tail of the events and therefore might obtain the endpoint at 1150 GeV. This suggests that the region of the fit must be chosen carefully. In particular, the events near the fitted endpoint must make up a sizable fraction of the total events. For points b, d and f, we first fit the region from the m_{T2} slightly above the peak position of the distribution up to the highest bin with enough statistics (> 10 events/bin). We then increase the lower limit until we obtain a small $\Delta\chi^2$. The $\Delta\chi^2$/n.d.f is less than 1 except at points c and e, and all fits satisfy $\Delta\chi^2/{\rm n.d.f} < 2$.

We now demonstrate the gluino mass determination using the endpoint of the $m_{T2}^{\rm sub}$ distribution. Here we must pay some attention to reduce the contributions from the squark-squark pair productions, which give the endpoints of the $m_{T2}^{\rm sub}$ distribution as $m_{\tilde{q}}$. This contribution smears the endpoint at the gluino mass. It is important to find the cuts to reduce the events.

We find that the cut on the number of high p_T jets above a certain threshold is useful to reduce the contamination, becuase the squark decay tends to give high p_T jets, as we have discussed earlier. To see this, we first show the distributions of the highest p_T jet at point a for 50,000 generated events in figure 7. The solid lines show the $p_T(1st)$ distribution, where $p(1st)$ is the momentum of the highest p_T jet among the jets with $|\eta| < 3$. The dashed lines show the contribution from the events with $n_{300} \equiv N_{\rm jet}(p_T > 300\,{\rm GeV}, |\eta| < 3) = 1$ and

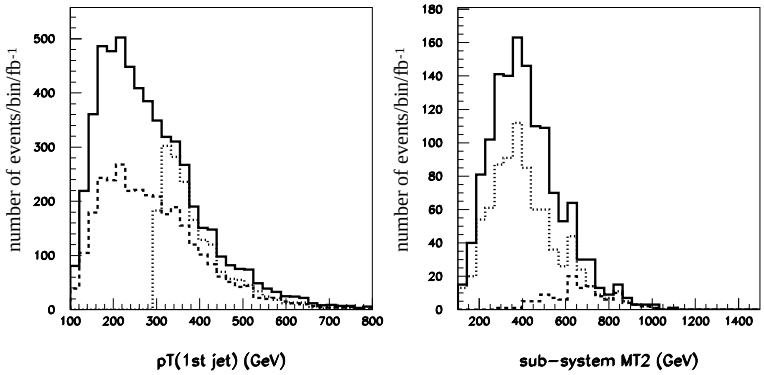

Figure 8: The same as figure 7 but at point f.

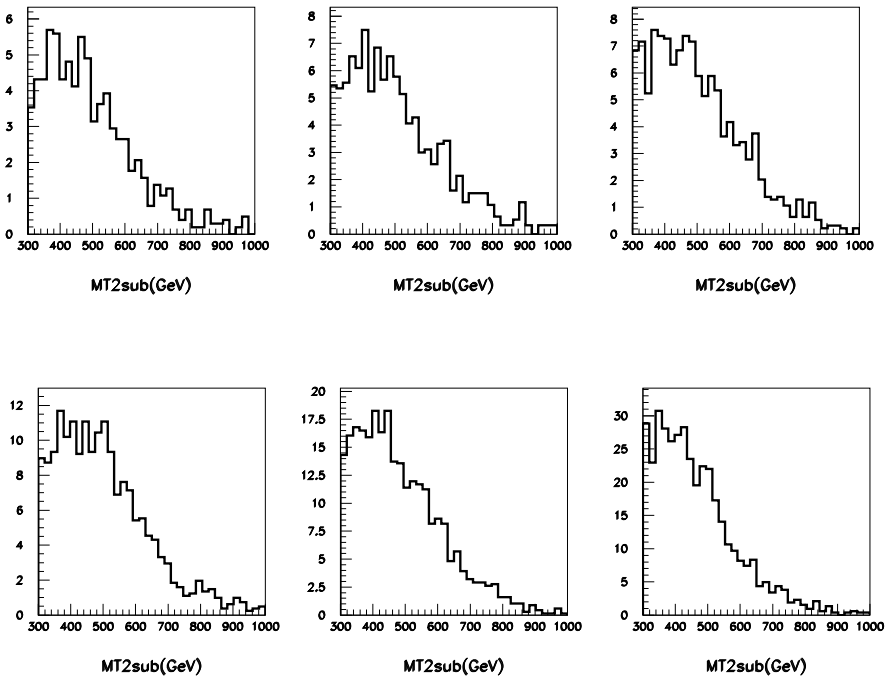

Figure 9: The $m_{T2}^{\rm sub}$ destributions at points a to f normalized for $1\,{\rm fb}^{-1}$. The input gluino masses differ slightly among the model points as we fix gaugino mass at the GUT scale. The top figures correspond to points a, b and c from left to right, and $m_{\tilde{g}} = 796, 785$, and $780\,{\rm GeV}$ respectively. The bottom figures correspond to points d, e and f, and $m_{\tilde{g}} = 773, 762$ and $745\,{\rm GeV}$. The squark mass is $1516\,{\rm GeV}$ at point a and $881\,{\rm GeV}$ at point f.

the dotted lines show the contributions of the events with $n_{\tilde{q}} = 1$, where $n_{\tilde{q}}$ is the number of primary produced 1st generation squarks of the events. The standard SUSY cuts are applied to the events. We can see that most of the events with $p_T(1st) > 300\,{\rm GeV}$ satisfy

JHEP10(2008)100

$n_{300} = 1$ and they mostly come from squark-gluino productions. Therefore, if $n_{300} \geq 2$, they are likely come from squark-squark pair production events.

Based on the above observation, we calculate the $m_{T2}^{\rm sub}$ distribution only for the events which have only one or zero high p_T jet above a certain p_T threshold. The actual value of the p_T cut should be chosen based on the signal distribution. For our model points, we take the cut $n_{300} \leq 1$. We do not include the events with $n_{300} \geq 2$, because our MC simulations show that they mostly come from the squark pair production. In the right figure, we show $m_{T2}^{\rm sub}$ distributions for the events $n_{300} = 1$ at point a. The dotted line shows the distribution with $n_{300} = 1$ and $n_{\tilde{q}} = 1$. The dashed line is the distribution with $m_{T2} > 800\,\text{GeV}$, $n_{300} = 1$ and $n_{\tilde{q}} = 1$. All distributions show the $m_{T2}^{\rm sub}$ endpoint close to the gluino mass value $\sim 800\,\text{GeV}$, which is expected from the parton level analysis.

Figure 8 shows the same distributions at point f. Events from squark-gluino co-production still dominate the events with $p_T > 300\,\text{GeV}$, and a significant fraction of the events satisfy $n_{300} = 1$. The events near the $m_{T2}^{\rm sub}$ endpoint mostly come from squark-gluino production. The endpoint of the distribution $\sim 750\,\text{GeV}$ is consistent with the gluino mass.

The $m_{T2}^{\rm sub}$ distributions at points a to f for $1\,\text{fb}^{-1}$ of integrated luminosity are shown in figure 9. Here we require $n_{300} \leq 1$; therefore, the distributions now include significant events from gluino-gluino production unlike the previous plots. We have seen that the m_{T2} distribution changes significantly among points a to f. The $m_{T2}^{\rm sub}$ distributions are, by contrast, similar. This is because the $m_{T2}^{\rm sub}$ endpoints must be very close to the true gluino mass $m_{\tilde{g}} \sim 750\,\text{GeV}$ (up to the difference of the test LSP mass from the true LSP mass). This is also seen in figure 6, where the value of the fitted $m_{T2}^{\rm sub}$ endpoint is shown together with the gluino mass for each point.

4. Background m_{T2} and $m_{T2}^{\rm sub}$ distributions

The Standard Model background to the SUSY processes has been studied by ATLAS and CMS groups extensively. The ratio $\not{E}_T / M_{\rm eff}$ gives a good discrimination between the SUSY signal and the background. In the previous section we required $\not{E}_T / M_{\rm eff} > 0.2$ in addition to $M_{\rm eff} > 500\,\text{GeV}$ and $\not{E}_T > 200\,\text{GeV}$.

The production cross section of the SM background is huge compared with the typical signal cross section. To measure the endpoint of the signal m_{T2} and $m_{T2}^{\rm sub}$ distributions, the signal to noise ratio (S/N) must be sufficiently small near the endpoint. The SM backgrounds in the 0-lepton channel after the standard SUSY cuts come from the four different sources: $t\bar{t}$, $W^{\pm}$, Z^0 productions with multiple jets, and QCD multi-jet processes. Bottom quark productions and the mis-measurements of particle energies can give the missing energy to QCD multi-jet processes. It is difficult to estimate the QCD background without knowing detector performances in detail. We therefore do not attempt to do so in this paper. In recent ATLAS and CMS studies [17], the four channels contribute to the background at roughly the same order of magnitude after the cuts to reduce the SM backgrounds, although QCD background decreases much faster with increasing $M_{\rm eff}$.

The source of missing E_T for the processes $t\bar{t}$, Z^0, and $W^{\pm}+n$ jets is primarily escaping neutrinos, and missing E_T arising from energy mis-measurements is less important. We

JHEP10(2008)100

	$t\bar{t}$	W	Z	total
$m_{T2} > 500\,\mathrm{GeV}$	77.7	104.9	107.0	289.6
	38.4	44.8	39.9	123.1
$m_{T2} > 700\,\mathrm{GeV}$	20.3	24.4	23.4	68.2
	10.0	12.0	10.4	32.4
$m_{T2}^{\mathrm{sub}} > 300\,\mathrm{GeV}$	90.3	80.4	82.2	252.9
	44.2	38.5	31.7	113.1
$m_{T2}^{\mathrm{sub}} > 500\,\mathrm{GeV}$	11.1	6.9	6.1	24.0
	8.1	4.9	3.8	16.8
luminosity	$13.1\,\mathrm{fb}^{-1}$	$13.5\,\mathrm{fb}^{-1}$	$19.1\,\mathrm{fb}^{-1}$	

Table 3: Number of SM background events per $1\,\mathrm{fb}^{-1}$. For each row, upper (lower) numbers correspond to the events without (with) a cut on the hemisphere masses, $m_{\mathrm{hemi}} > 200\,\mathrm{GeV}$. The last row shows the number of generated events for this study in terms of the corresponding integrated luminosity.

generate these events using ALPGEN [28, 29], and parton shower and initial state radiations are estimated by interfacing the parton level events to HERWIG. We generate $Z^0(\to \nu\bar{\nu}) + n$ jets for $n \leq 5$, $W^{\pm}(\to l\nu) + n$ jets $(n \leq 4)$, and $t\bar{t} + n$ jets $(n \leq 2)$, so that tree level 0 lepton events have at least 4 or 5 jets including τ jets. We require minimum parton separation $\Delta R_{jj} > 0.6$,[4] and place a cut on the forward parton of $|\eta| < 5$. The events are then matched so that there is no double counting between parton shower and hard partons by using the MLM matching scheme provided by ALPGEN. In this scheme, we generate the processes with up to n_{max} parton. The events from the processes with n partons $(n < n_{\mathrm{max}})$ are accepted only if jets and partons match $(n_{\mathrm{jet}} = n)$, while the events from the processes with n_{max} partons are accepted if $n_{\mathrm{jet}} \geq n$. In order to reduce the number of produced events while keeping enough statistics for the kinematical region we are interested in, we require $\sum_{\mathrm{parton}} E_T > 400\,\mathrm{GeV}$ for $W+$ n jets, $\not{E}_T > 150\,\mathrm{GeV}$ for $Z+n$ jets, $\sum_{\mathrm{parton}} E_T > 500\,\mathrm{GeV}$ for $t\bar{t}+$ n jets.[5] The effect of additional jets on the signal distributions is small and discussed in appendix B.

AcerDET performs Gaussian smearing for jet momenta, the missing momentum, and isolated lepton momenta. It does not contain various potentially important instrumental effects, such as non-Gaussian tails of the energy smearing and lepton inefficiencies. Therefore, our background estimate is given in this paper for illustrative purpose, and more realistic estimates must be performed by the experimental groups.

Keeping this in mind, table 3 summarizes results of our event generations. The number of background events for $\int dt\mathcal{L} = 1\,\mathrm{fb}^{-1}$ under various cuts are given. The bottom row shows the corresponding luminosities we have generated for the background processes.

[4]The jet cone size for AcerDET jet reconstruction is set to $R = 0.4$. This means that centers of two well separated jets has $\Delta R > 0.8$. We therefore require ΔR_{jj} to be slightly lower than that. This is sufficient for our purpose as we are working on inclusive signatures. Reducing the ΔR_{jj} cut to less than 0.6 results in unnecessary inefficiency to the event generation.

[5]The conditions of the generations for the different processes are not the same. However, these conditions are loose enough so that there is no effect of the generation cuts after our standard SUSY cuts.

JHEP10(2008)100

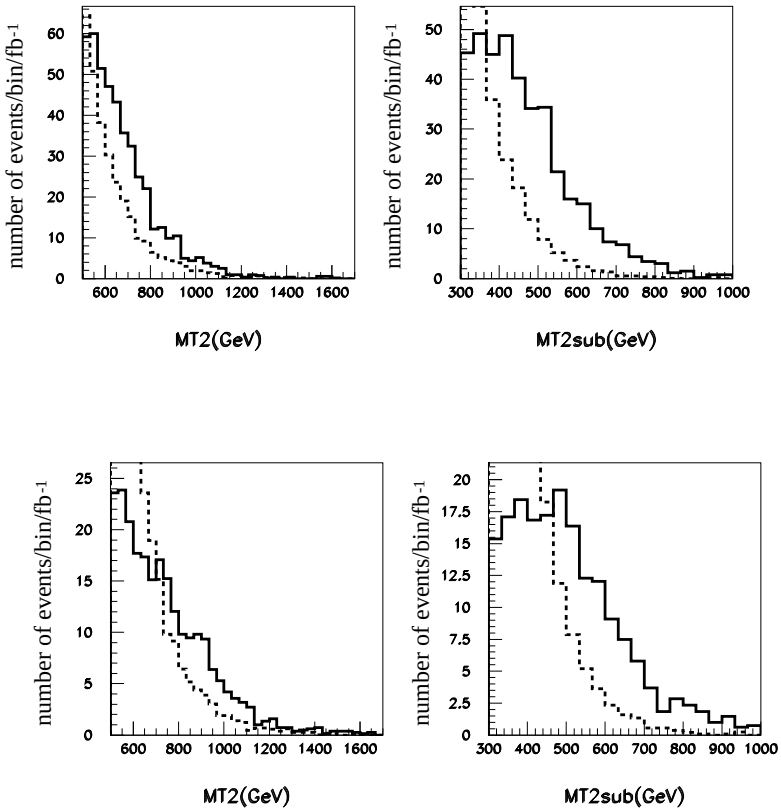

Figure 10: Signal and background distributions at point f (the top figures) and at point d (the bottom figures). Unit of y-axes is events/bin/1 fb^{-1}.

We apply the SUSY cuts given in section 4. In addition, we require $n_{300} \leq 1$ for $m_{T2}^{\rm sub}$ distribution. We do not include K factors, as the corresponding higher order QCD corrections are not available. Note that K factors of $t\bar{t}$ production and SUSY production tend to cancel partially. For each row, upper (lower) numbers correspond to the events without (with) a cut on the hemisphere masses, $m_{\rm hemi} > 200\,{\rm GeV}$. The background with the hemisphere mass cut is reduced by more than a factor of 2. This suggests that the background events are dominated by the configurations that a few jets are either soft or colinear to leading hard jets and therefore the masses of the hemispheres are small. The background distributions will be studied in detail elsewhere.

Figure 10 shows the distribution of background, together with the signal distribution at points f (the top figures) and d (the bottom figures). These distributions are without hemisphere mass cuts. The signal is larger than the background above $m_{T2} > 600$ (750) GeV at points f (d) for the m_{T2} distribution, which is much smaller than expected $m_{T2}^{\rm end} = m_{\tilde{q}} = 881\,{\rm GeV}$ ($1175\,{\rm GeV}$). The endpoints of the signal m_{T2} and $m_{T2}^{\rm sub}$ distributions may be extracted as a kink in the total distribution in this case. The signal and background distributions of $m_{T2}^{\rm sub}$ are also shown in the right plots. Again, the level of the background is small near the endpoint.

JHEP10(2008)100

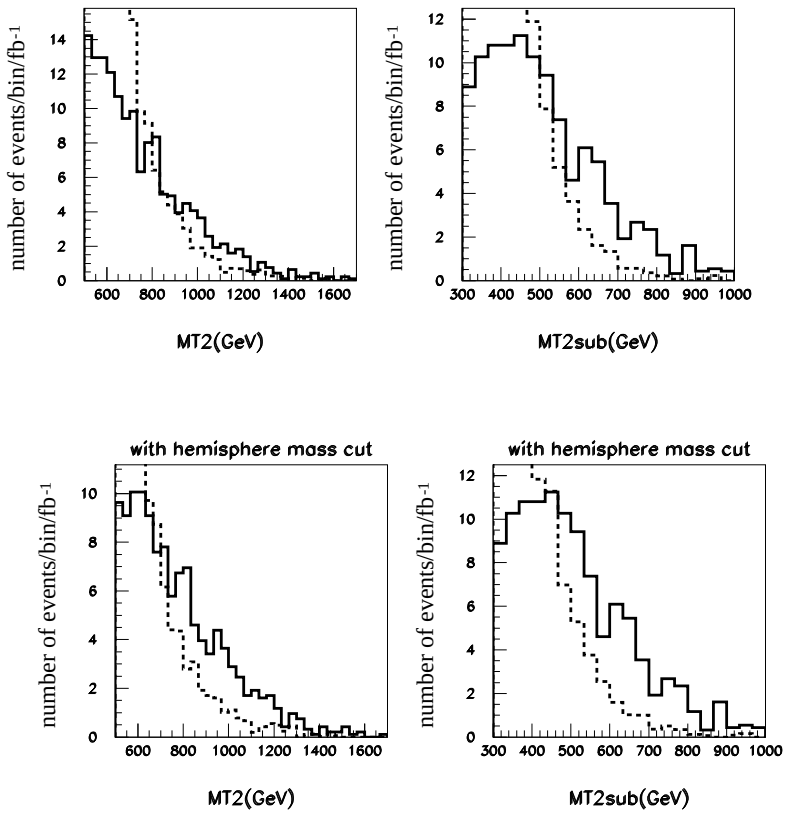

Figure 11: The signal (solid) and background (dashed) distributions at point b. The bottom figures show the distributions with the hemisphere mass cut $m_{\rm hemi}^{1(2)} > 200\,{\rm GeV}$. Unit of y-axes is events/bin/$1\,{\rm fb}^{-1}$.

We also show the same distribution at point b in figure 11. The signal cross section involving $\tilde{q}$ production is reduced by a factor of 1/5 from that at point f (See table 2). The S/N above $m_{T2} > 700\,{\rm GeV}$ is now ~ 1 and the cross point of the signal and the background is at $m_{T2} = 800\,{\rm GeV}$. By applying the hemisphere mass cut, we can reduce the background significantly. The improvement of S/N near the endpoint can be seen by comparing the top and bottom figures without/with the hemisphere mass cut. It is important to reduce the background to measure the squark and gluino masses near the discovery regions.

5. Conclusions

The ATLAS and CMS experiments at the LHC can discover squarks and gluinos in the MSSM with masses less than 1.5 TeV at the early stage of the experiment with luminosity around $\int dt\mathcal{L} = 1\,{\rm fb}^{-1}$. Developing a reliable method of estimating squark and gluino masses with the discovery is an important step to study supersymmetry at the LHC.

For this purpose we cannot rely on the clean golden channels such as $l^{\pm}l^{\mp}+$ jets,

JHEP10(2008)100

becuase they tend to have small branching ratios and are sensitive to the model parameters. In a previous paper [22], we defined an inclusive m_{T2} variable. This variable can be calculated for any event with jets and missing transverse energy. It is calculated in two steps; we first define the two hemisphere axes by assigning particles into the two leading jets of the events, then, the m_{T2} variable is caluculated from the two hemisphere momenta and missing transverse energy. We pointed out that the endpoint of the m_{T2} distribution is sensitive to the squark mass for the case $m_{\tilde{q}} > m_{\tilde{g}}$.

In this paper, we define a "sub-system" m_{T2}, $m_{T2}^{\rm sub}$. This is an m_{T2} variable calculated without including the highest p_T jets for the hemisphere assignments and m_{T2} calculation. In the case that $m_{\tilde{q}} > m_{\tilde{g}}$ and the other sparticles are lighter, the endpoint of $m_{T2}^{\rm sub}$ distribution gives us information on $m_{\tilde{q}}$. In this paper, we show convincing evidence for sample model points within the reach for $\int dt\mathcal{L} = 1{\rm fb}^{-1}$.

We also provide various parton level checks on the hemisphere algorithm. We estimate background distributions arising from $t\bar{t}$+n jets, Z^0+ n jets and $W^{\pm}$ + n jets using `ALPGEN` and find out that S/N ratio is large for the events near the m_{T2} endpoints at our sample points. In the appendix, we also provide a study of SUSY+n jet distributions using `MadGraph/MadEvent`, and find that the endpoint is stable with the ME corrections.

Acknowledgments

We would like to thank to Rikkert Frederix for help with using Madgraph and to Willie Klemm for careful reading of the manuscript. This work is supported in part by World Premier International Research Center InitiativeiWPI Initiative), MEXT, Japan,. M.M.N. and K.S. are supported in part by the Grant-in-Aid for Science Research,MEXT, Japan .

A. The m_{T2} endpoint for squark-gluino production events

In this appendix, we show the condition for which the endpoint of the ideal m_{T2} distribution for the squark-gluino production events coincides with the squark mass at $M_{\rm test} = m_{\rm LSP}$.

The squark-gluino m_{T2} is calculated by minimizing $\max\{m_T^{(\tilde{q})}, m_T^{(\tilde{g})}\}$ under the condition that the sum of transverse test momenta of two LSP is equal to the $\not{E}_T$. It is known that the transverse mass $m_T^{(i)}$ $(i = \tilde{q}, \tilde{g})$ as a function of the test LSP momentum has the global minimum, which is called the *unconstrained minimum* (UCM) [15]. There are cases where m_{T2} is given by the *unconstrained minimum* of the transverse mass on one side $(m_T^{(i)})_{\rm UCM}$. This situation occurs when $m_T^{(j)}$ on the other side for the test LSP momentum which gives the $(m_T^{(i)})_{\rm UCM}$ is smaller than $(m_T^{(i)})_{\rm UCM}$.

In ref. [18], it is shown that the UCM of the squark system $((m_T^{(\tilde{q})})_{\rm UCM})$ is given by

$$(m_T^{(\tilde{q})})_{\rm UCM} = m_{\rm vis}^{(\tilde{q})} + M_{\rm test}, \tag{A.1}$$

where $m_{\rm vis}^{(\tilde{q})}$ is the invariant mass of the visible particles from the squark decay. The maximum of $(m_T^{(\tilde{q})})_{\rm UCM}$ is, therefore, given by substituting the maximum of $m_{\rm vis}^{(\tilde{q})}$ into eq. A.1. The maximum of the $m_{\rm vis}^{(\tilde{q})}$ is given by

$$(m_{\rm vis}^{(\tilde{q})})^{\rm max} = m_{\tilde{q}} - m_{\rm LSP}, \tag{A.2}$$

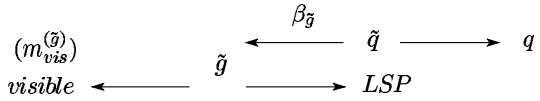

Figure 12: A Kinematical configuration of squark decay

if the LSP from squark decay can be at rest in the squark rest frame. In this case, the maximum of the UCM of the squark system can reach the squark mass at $M_{\rm test} = m_{\rm LSP}$, and the maximum of the squark-gluino m_{T2} is identical to the squark mass at $M_{\rm test} = m_{\rm LSP}$.

We now consider the condition that the LSP can be at rest in the squark rest frame. In the following discussion, we concentrate on the case that the squark decays into the gluino and a jet. The gluino from the squark subsequently decays into the visible objects and the LSP (See figure 12). The LSP momentum in the gluino rest frame ($p'_{\rm LSP}$) depends on the invariant mass of the visible objects ($m_{\rm vis}^{(\tilde{g})}$) as

$$|p'_{\rm LSP}| = \frac{1}{2m_{\tilde{g}}}\sqrt{m_{\tilde{g}}^4 - 2m_{\tilde{g}}^2((m_{\rm vis}^{(\tilde{g})})^2 + m_{\rm LSP}^2) + ((m_{\rm vis}^{(\tilde{g})})^2 - m_{\rm LSP}^2)^2} \quad . \tag{A.3}$$

If the LSP is produced in the opposite direction from the gluino momentum and the gluino velocity is not too large, the LSP can be at rest in the squark rest frame for a suitable value of the invariant mass of the visible objects ($\tilde{m}_{\rm vis}^{(\tilde{g})}$). In this situation, the LSP momentum in the squark rest frame ($p_{\rm LSP}$) is obtained by the Lorentz boost of the $p'_{\rm LSP}$ as

$$p_{\rm LSP} = \gamma_{\tilde{g}}(-|\beta_{\tilde{g}}|E'_{\rm LSP} + |p'_{\rm LSP}|)\,, \tag{A.4}$$

where $E'_{\rm LSP}$ is the energy of the LSP in the gluino rest frame, and the Lorentz boost factors $\beta_{\tilde{g}}$ and $\gamma_{\tilde{g}}$ are given by

$$|\beta_{\tilde{g}}| = \frac{m_{\tilde{q}}^2 - m_{\tilde{g}}^2}{m_{\tilde{q}}^2 + m_{\tilde{g}}^2}, \qquad \gamma_{\tilde{g}} = 1/\sqrt{1-\beta_{\tilde{g}}^2} = \frac{m_{\tilde{q}}^2 + m_{\tilde{g}}^2}{2m_{\tilde{q}}m_{\tilde{g}}}. \tag{A.5}$$

By solving the equation $p_{\rm LSP} = 0$, we obtain

$$(\tilde{m}_{\rm vis}^{(\tilde{g})})^2 = m_{\tilde{g}}^2\left(1 - \frac{m_{\rm LSP}}{m_{\tilde{q}}}\right)\left(1 - \frac{m_{\tilde{q}}m_{\rm LSP}}{m_{\tilde{g}}^2}\right)\,. \tag{A.6}$$

Note that if $m_{\tilde{q}}m_{\rm LSP} > m_{\tilde{g}}^2$, the equation $p_{\rm LSP} = 0$ does not have any solution for positive $\tilde{m}_{\rm vis}^{(\tilde{g})}$. In this case, the LSP cannot be at rest in the squark rest frame, and $(m_T^{(\tilde{q})})_{\rm UCM}$ is less than the squark mass. Even if the equation $p_{\rm LSP} = 0$ has a solution for positive $\tilde{m}_{\rm vis}^{(\tilde{g})}$, there are cases where $m_{\rm vis}^{(\tilde{g})}$ has a non-vanishing kinematical lower bound due to a heavy standard model particle, such as t, Z and W. If the lower bound is smaller than the solution $\tilde{m}_{\rm vis}^{(\tilde{g})}$, $(m_T^{(\tilde{q})})_{\rm UCM}$ cannot reach the squark mass. For our model points, the solution (A.6) is $\tilde{m}_{\rm vis}^{(\tilde{g})}/m_{\tilde{g}} = 0.83$ for point a, and $\tilde{m}_{\rm vis}^{(\tilde{g})}/m_{\tilde{g}} = 0.85$ for point f. On the other hand, the kinematically allowed range of the visible invariant mass is roughly $0.50 \leq m_{\rm vis}^{(\tilde{g})}/m_{\tilde{g}} \leq 0.86$ for point a, and $0.55 \leq m_{\rm vis}^{(\tilde{g})}/m_{\tilde{g}} \leq 0.86$ for point f. Therefore, the endpoint of the ideal m_{T2} distribution in the squark-gluino production events is identical to the squark mass in our model points.

JHEP10(2008)100

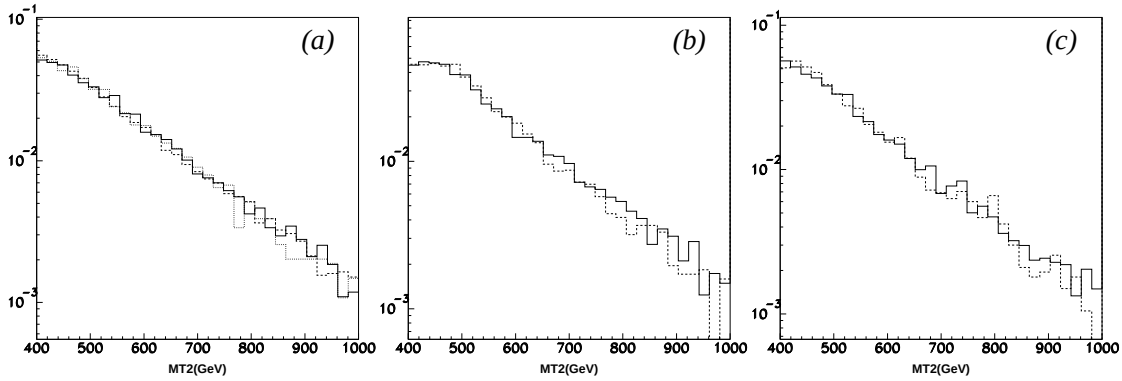

Figure 13: (a) m_{T2} distributions for $\tilde{g}\tilde{g}$ +0 jet (dashed), 1 jet (solid) 2 jets (dotted). (b) m_{T2} distributions for $\tilde{q}\tilde{q}$ +0 jet (solid), 1 jet (dashed). (c) m_{T2} distributions for $\tilde{g}\tilde{q}$ +0 jet (solid), 1 jet (dashed). Here SUSY spectrum is assumed as SPS 1a.

B. The effect of matrix element corrections to the signal distribution

In this appendix we consider the matching effect of multi-jet matrix elements (ME) and parton showers on the m_{T2} distribution. When we calculate the signal m_{T2} distributions in this text, we generate SUSY processes at the lowest-order hard process and then generate multi-jet events by parton showers. In general, there are ME corrections from hard parton emissions in the lowest order hard process, which may not be included in the parton shower approach. Note that we have applied cuts $p_T > 50\,\text{GeV}$ and $|\eta| < 3$ for the jets to be included in the hemispheres. We need to check that this is enough to kill the effects of initial state radiations.

When the ME corrections are taken into account, we should avoid double counting of emissions in overlapping phase space and need some kind of matching scheme to merge the ME corrections. Here, we study the ME corrections using the `MadGraph /MadEvent` MC generator [33], in which the matching between the ME corrections and the parton showers is implemented. For our analysis, we use a modified MLM matching procedure with $k_\perp$ jets. In this scheme, the parton emissions are separated into two phase space regions at some $k_\perp$. In `MadGraph/MadEvent`, only events with enough separated partons, $k_\perp >$ xqcut, are generated after the matrix element simulation. Then parton showering is performed and the partons are clustered into jets using the $k_\perp$ algorithm. After this procedure, the matching between the jets and the partons from the matrix elements is performed using Pythia. If the distance between them is larger than Qcut, the event is discarded in order to avoid double counting.

In order to see the effect of the additional jet emission, we generate the SUSY events for the mSUGRA point SPS 1a using `MadGraph/MadEvent`. The generated parton level events are interfaced with Pythia to take into account the matching and the hadronization. We take the matching parameters as xqcut= 40 GeV, Qcut= 60 GeV. After hadronic events are generated, we use `AcerDET` for detector simulations. We apply the same cuts given in the section 4 to select the events.

In figure 13(a), we plot the m_{T2} distributions for gluino pair-production processes with

0, 1, 2 jets. Since the total cross sections could receive large NLO corrections, the shape of m_{T2} distribution is more important. For comparison, we normalize the each distribution to unity. We can see that the shapes of the m_{T2} distributions are stable against the ME corrections. This is a good feature to obtain information on the gluino mass from the endpoint of the m_{T2} distributions.

In figure 13(b) and 12(c), we plot the m_{T2} distributions for squark pair-production (squark-gluino) processes with 0, 1 jet. We also normalize each distribution to unity. Again we can see that the m_{T2} distributions are rather insensitive to the ME corrections and the matching.

References

[1] H.P. Nilles, *Supersymmetry, supergravity and particle physics*, *Phys. Rept.* **110** (1984) 1.

[2] H.E. Haber and G.L. Kane, *The search for supersymmetry: probing physics beyond the standard model*, *Phys. Rept.* **117** (1985) 75.

[3] S.P. Martin, *A supersymmetry primer*, hep-ph/9709356.

[4] I. Hinchliffe, F.E. Paige, M.D. Shapiro, J. Soderqvist and W. Yao, *Precision SUSY measurements at LHC*, *Phys. Rev.* **D 55** (1997) 5520 [hep-ph/9610544].

[5] CMS collaboration, S. Abdullin et al., *Discovery potential for supersymmetry in CMS*, *J. Phys.* **G 28** (2002) 469 [hep-ph/9806366].

[6] ATLAS collaboration, *ATLAS: detector and physics performance technical design report. Volume* 1, CERN-LHCC-99-14 (1999); *ATLAS: detector and physics performance technical design report. Volume* 2, CERN-LHCC-99-15 (1999).

[7] H. Bachacou, I. Hinchliffe and F.E. Paige, *Measurements of masses in SUGRA models at LHC*, *Phys. Rev.* **D 62** (2000) 015009 [hep-ph/9907518].

[8] I. Hinchliffe and F.E. Paige, *Measurements in SUGRA models with large* $\tan\beta$ *at LHC*, *Phys. Rev.* **D 61** (2000) 095011 [hep-ph/9907519].

[9] B.C. Allanach, C.G. Lester, M.A. Parker and B.R. Webber, *Measuring sparticle masses in non-universal string inspired models at the LHC*, *JHEP* **09** (2000) 004 [hep-ph/0007009].

[10] M.M. Nojiri, G. Polesello and D.R. Tovey, *Proposal for a new reconstruction technique for SUSY processes at the LHC*, hep-ph/0312317.

[11] K. Kawagoe, M.M. Nojiri and G. Polesello, *A new SUSY mass reconstruction method at the CERN LHC*, *Phys. Rev.* **D 71** (2005) 035008 [hep-ph/0410160].

[12] M.M. Nojiri, G. Polesello and D.R. Tovey, *A hybrid method for determining SUSY particle masses at the LHC with fully identified cascade decays*, *JHEP* **05** (2008) 014 [arXiv:0712.2718].

[13] H.-C. Cheng, D. Engelhardt, J.F. Gunion, Z. Han and B. McElrath, *Accurate mass determinations in decay chains with missing energy*, *Phys. Rev. Lett.* **100** (2008) 252001 [arXiv:0802.4290].

[14] C.G. Lester and D.J. Summers, *Measuring masses of semi-invisibly decaying particles pair produced at hadron colliders*, *Phys. Lett.* **B 463** (1999) 99 [hep-ph/9906349].

JHEP10(2008)100

[15] A. Barr, C. Lester and P. Stephens, *m_{T2}: the truth behind the glamour*, *J. Phys.* **G 29** (2003) 2343 [hep-ph/0304226].

[16] LHC/LC Study Group collaboration, G. Weiglein et al., *Physics interplay of the LHC and the ILC*, *Phys. Rept.* **426** (2006) 47 [hep-ph/0410364].

[17] O. Brandt, *SUSY searches at the LHC*, talk in *Hadron Collider Physics Symposium* 2008 *(HCP)*, Galena U.S.A. May 27–31 2008.

[18] W.S. Cho, K. Choi, Y.G. Kim and C.B. Park, *Gluino stransverse mass*, *Phys. Rev. Lett.* **100** (2008) 171801 [arXiv:0709.0288].

[19] B. Gripaios, *Transverse observables and mass determination at hadron colliders*, *JHEP* **02** (2008) 053 [arXiv:0709.2740].

[20] A.J. Barr, B. Gripaios and C.G. Lester, *Weighing wimps with kinks at colliders: invisible particle mass measurements from endpoints*, *JHEP* **02** (2008) 014 [arXiv:0711.4008].

[21] W.S. Cho, K. Choi, Y.G. Kim and C.B. Park, *Measuring superparticle masses at hadron collider using the transverse mass kink*, *JHEP* **02** (2008) 035 [arXiv:0711.4526].

[22] M.M. Nojiri, Y. Shimizu, S. Okada and K. Kawagoe, *Inclusive transverse mass analysis for squark and gluino mass determination*, *JHEP* **06** (2008) 035 [arXiv:0802.2412].

[23] A.J. Barr, G.G. Ross and M. Serna, *The precision determination of invisible-particle masses at the LHC*, *Phys. Rev.* **D 78** (2008) 056006 [arXiv:0806.3224].

[24] D.R. Tovey, *On measuring the masses of pair-produced semi-invisibly decaying particles at hadron colliders*, *JHEP* **04** (2008) 034 [arXiv:0802.2879].

[25] F. Moortgat and L. Pape, *CMS Physics TDR, vol. II*, Report No. CERN-LHCC-2006, section 13.4, pg.410.

[26] S. Matsumoto, M.M. Nojiri and D. Nomura, *Hunting for the top partner in the littlest Higgs model with T-parity at the LHC*, *Phys. Rev.* **D 75** (2007) 055006 [hep-ph/0612249].

[27] J. Hubisz, J. Lykken, M. Pierini and M. Spiropulu, *Missing energy look-alikes with* $100\,pb^{-1}$ *at the LHC*, *Phys. Rev.* **D 78** (2008) 075008 [arXiv:0805.2398].

[28] M.L. Mangano, M. Moretti, F. Piccinini, R. Pittau and A.D. Polosa, *ALPGEN, a generator for hard multiparton processes in hadronic collisions*, *JHEP* **07** (2003) 001 [hep-ph/0206293].

[29] M.L. Mangano, M. Moretti and R. Pittau, *Multijet matrix elements and shower evolution in hadronic collisions: $Wb\bar{b}$+ (n)jets as a case study*, *Nucl. Phys.* **B 632** (2002) 343 [hep-ph/0108069].

[30] T. Plehn, D. Rainwater and P. Skands, *Squark and gluino production with jets*, *Phys. Lett.* **B 645** (2007) 217 [hep-ph/0510144].

[31] J. Alwall, *New developements in MagGraph/MadEvent*, talk in *The* 16^{th} *International Confernce on Supersymmetry and the Unification of Fundamental Interactions, (SUSY*08*)*, Seoul Korea June 16–21 2008.

[32] J. Alwall, M.-P. Le, M. Lisanti and J.G. Wacker, *Searching for gluinos at the tevatron*, *Phys. Rev. Lett.* **B666** (2008) 34 [arXiv:0803.0019].

[33] J. Alwall et al., *MadGraph/MadEvent v*4*: the new web generation*, *JHEP* **09** (2007) 028 [arXiv:0706.2334].

JHEP10(2008)100

[34] G. Corcella et al., *HERWIG* 6*: an event generator for hadron emission reactions with interfering gluons (including supersymmetric processes)*, *JHEP* **01** (2001) 010 [hep-ph/0011363]; *HERWIG* 6.5 *release note*, hep-ph/0210213.

[35] E. Richter-Was, *AcerDET: a particle level fast simulation and reconstruction package for phenomenological studies on high p_T physics at LHC*, hep-ph/0207355.

[36] M. Drees et al., *Scrutinizing LSP dark matter at the LHC*, *Phys. Rev.* **D 63** (2001) 035008 [hep-ph/0007202].

[37] J.R. Ellis, K.A. Olive and Y. Santoso, *The MSSM parameter space with non-universal Higgs masses*, *Phys. Lett.* **B 539** (2002) 107 [hep-ph/0204192].

[38] J.R. Ellis, T. Falk, K.A. Olive and Y. Santoso, *Exploration of the MSSM with non-universal Higgs masses*, *Nucl. Phys.* **B 652** (2003) 259 [hep-ph/0210205].

[39] F.E. Paige, S.D. Protopopescu, H. Baer and X. Tata, *ISAJET* 7.69*: a Monte Carlo event generator for pp, $\bar{p}p$ and e^+e^- reactions*, hep-ph/0312045.

[40] P. Richardson, *ISAWIG*, http://www.hep.phy.cam.ac.uk/∼richardn/HERWIG/ISAWIG/.

JHEP10(2008)100